ADVANCED ENERGY MATERIALS
www.advenergymat.de

A Pyrazinyl Wide-Bandgap Polymer Donor Yields 19.35% Efficiency in Tandem Organic Solar Cells

Huazhe Liang, Kangqiao Ma, Shuhui Ding, Wenkai Zhao, Xiaodong Si, Xiangjian Cao, Zhaoyang Yao, Tainan Duan, Guankui Long, Chenxi Li, Xiangjian Wan, and Yongsheng Chen**

In series-connected tandem organic solar cells (TOSCs), various light-harvesting molecules with complementary absorptions are explored with the aim of collaboratively utilizing solar light to the maximum extent. In sharp contrast to the small molecular acceptors that possessing almost the successively tunable bandgaps, high-performance wide-bandgap (WBG) polymer donors in TOSCs are quite scarce, with only PM6 (optical bandgaps, E_g^{opt} = 1.80 eV) and D18 (E_g^{opt} = 1.98 eV) being widely used. Herein, to develop WBG polymer donors with large open-circuit voltages (V_{OC}) and high-energy photon absorption, two pyrazinyl polymer donors, PPy1 and PPy2, are synthesized with branched 2-butyloctyl and n-dodecyl chains on polymeric backbones, respectively, demonstrating the downshifted highest occupied molecular orbital energy levels of ≈−5.60 eV and thus afford E_g^{opt} over 2.0 eV. Consequently, when blending with a WBG acceptor F-ThCl, PPy2:F-ThCl-based devices exhibit a higher power conversion efficiency (PCE) of 14.50% and fill factor of 77.66%. In light of its large V_{OC} of 1.07 V, TOSCs based on PPy2 are further fabricated and exhibit an impressive PCE of 19.35% by using a narrow bandgap blend of PM6:CH1007:F-2F as a rear cell. This work demonstrates the great potential of pyrazine units in constructing WBG polymer donors for achieving record-breaking TOSCs.

1. Introduction

As a new generation of clean energy, organic solar cells (OSCs) have gained lots of interests owing to the remarkable advantages of flexibility, semitransparency, large-area print fabrication and so on.[1–6] Recently, power conversion efficiencies (PCEs) of OSCs have surpassed 20%,[7–11] but some inherent characteristics of organic materials restrict further improvements in efficiency. On the one hand, the intrinsic low carrier mobility of organic semiconductor materials generally limits the thickness of active layers, resulting in about 20–40% luminous flux loss.[12–13] On the other hand, more transmission loss and thermalization loss exist in single junction OSCs due to the limited absorption range of active layers.[14–15] Tandem organic solar cells (TOSCs) have been proved as an effective pathway to mitigate these constraints by connecting two or more sub-cells through an intermediate connection layer (ICL).[16–18] In series-connected TOSCs, wide-bandgap and narrow-bandgap molecules are selected as the active layer materials of front and rear sub-cells, respectively, to realize the collaborative utilization of absorption spectrum, which shows greater potential in achieving higher PCE.[19–20] Thus far, TOSCs have achieved 20.6% PCE via innovating new photovoltaic materials with complementary absorption, developing ICLs technology, and optimizing device fabrications.[21–22]

In particular, the development of highly efficient acceptor-donor-acceptor (A-D-A) type small molecule acceptors for both front and rear sub-cells plays a crucial role in promoting TOSCs.[14,17,19,23–24] For example, the emergence of Y-series molecular backbone can successfully regulate the absorption at a large range of 100 nm (absorption edges, λ_{onset} = 880–980 nm), making it highly promising application in the rear cell to effectively absorb the low-energy photons.[19,25–28] Meanwhile, plenty of high-performance acceptors with optical bandgaps (E_g^{opt}) >1.70 eV, such as F-ThBr,[14] AITC,[29] GS-ISO,[21] etc., have been extensively designed for front cells of TOSCs, which can utilize the high-energy photons to generate a large open circuit voltage (V_{OC}). However, the highly-efficient polymer donors are still

H. Liang, K. Ma, S. Ding, X. Si, X. Cao, Z. Yao, C. Li, X. Wan, Y. Chen
State Key Laboratory and Institute of Elemento-Organic Chemistry
The Centre of Nanoscale Science and Technology and Key Laboratory of Functional Polymer Materials
Renewable Energy Conversion and Storage Center (RECAST)
College of Chemistry
Nankai University
Tianjin 300071, China
E-mail: zyao@nankai.edu.cn; yschen99@nankai.edu.cn

W. Zhao, G. Long
School of Materials Science and Engineering
National Institute for Advanced Materials
Renewable Energy Conversion and Storage Center (RECAST)
Nankai University
Tianjin 300350, China

T. Duan
Chongqing Institute of Green and Intelligent Technology
Chongqing School
University of Chinese Academy of Sciences (UCAS Chongqing)
Chinese Academy of Sciences
Chongqing 400714, China

The ORCID identification number(s) for the author(s) of this article can be found under https://doi.org/10.1002/aenm.202402370

DOI: 10.1002/aenm.202402370

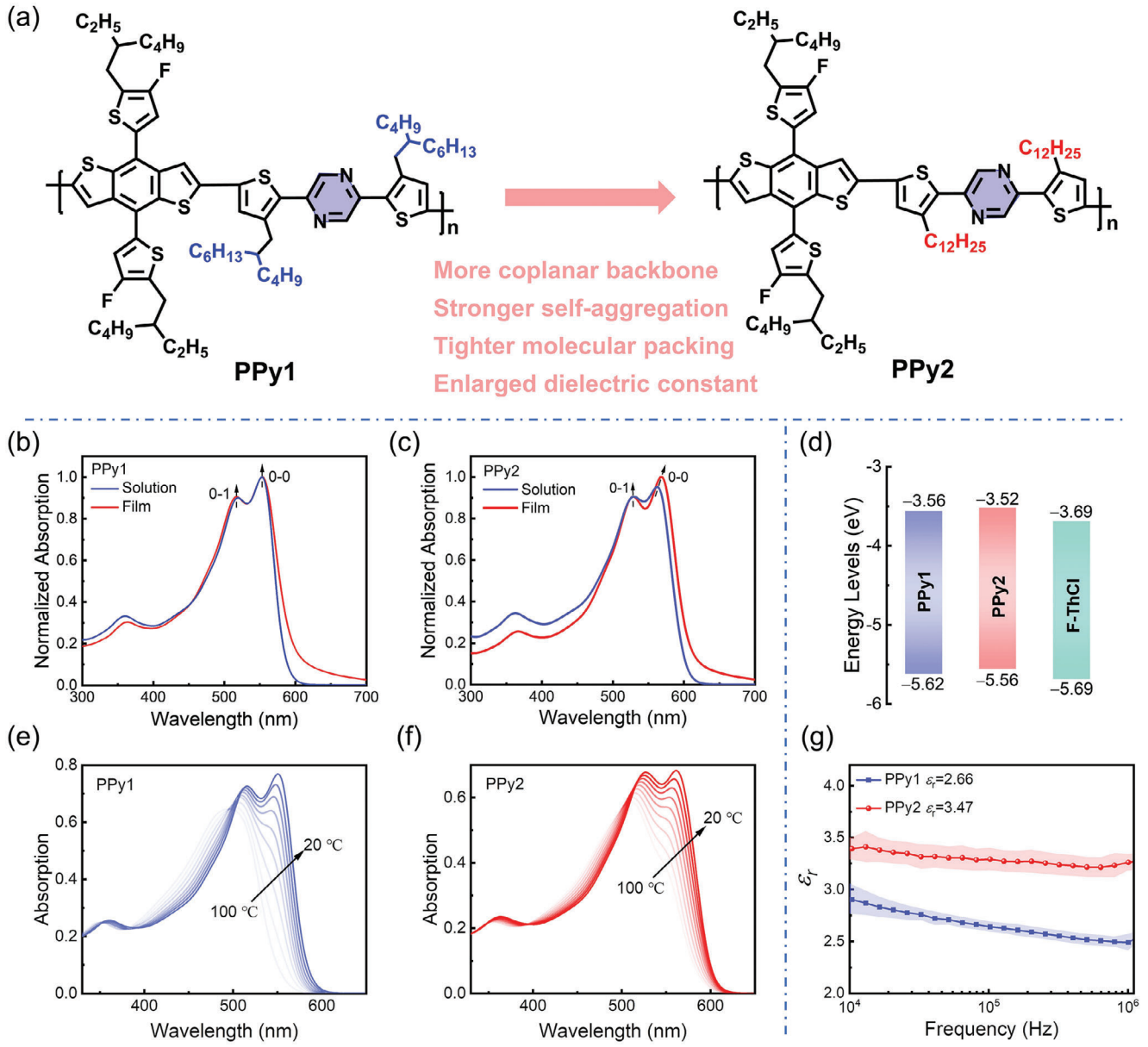

Figure 1. a) Molecular structures of PPy1 and PPy2. Normalized absorption spectra of b) PPy1 and c) PPy2 in solution and neat films. d) Energy level diagram. The absorption spectra of e) PPy1 and f) PPy2 in chlorobenzene solution with different temperatures. g) ε_r as a function of frequency.

limited on PM6,[30] D18[31] and its derivatives until now,[32,33] restricting the material selection in TOSCs and further application greatly. Therefore, the design and synthesis of new high-performance polymer donors for TOSCs and other application has become an urgent issue.[34–36] An excellent polymer donor for application in TOSCs requires wide-bandgap (WBG) and proper energy levels to absorb more high-energy photons, generate and improve the V_{OC}.[37–39] In front cells, developing polymer donors with E_g^{opt}s over 2.0 eV is necessary for achieving the coverage of the absorption spectrum from 450 to 730 nm.[17] Moreover, polymer donors should also possess the proper highest occupied molecular orbital (HOMO) and lowest unoccupied molecular orbital (LUMO) energy levels to match with WBG acceptors, so as to reduce energy losses under the condition of effective charge separation.[40–44]

As a well-known heterocyclic aromatic core with strong electronegativity, pyrazine unit has a great ability in effectively tailoring the structural and π-electron behaviors of polymers, which is suitable as A unit for D-A copolymerization to design WBG polymers.[39,45–48] Hence, two pyrazinyl polymer donors, PPy1 and PPy2 (**Figure 1a**), are synthesized with branched 2-butyloctyl and n-dodecyl chains on polymeric backbones, respectively. The two polymers show large E_g^{opt}s over 2.0 eV and suitable HOMO energy levels ≈−5.60 eV, well-matching the energy levels of WBG acceptor F-ThCl. As a result, PPy2:F-ThCl based OSCs yield a much-improved PCE of 14.50% with an excellent V_{OC} of 1.073 V

and fill factor (FF) of 77.66%, while PPy1:F-ThCl based devices only afford a PCE of 12.52%. Bearing its high V_{OC} and wide bandgap feature of PPy2:F-ThCl in mind, TOSCs were further constructed by employing PPy2:F-ThCl as a front cell and highly-efficient PM6:CH1007:F-2F system as a rear cell. The resulting TOSCs afford a remarkable PCE of 19.35%, highlighting the considerable potential of pyrazine unit for constructing high-performance WBG polymer donors in OSCs.

2. Results and Discussion

2.1. Physicochemical Properties

As shown in Scheme S1 (Supporting Information), the target polymers were achieved through Stille coupling polymerization between fluorinated-thienyl benzodithiophene (BDT-TF-Sn, monomer 5) and brominated monomer 4 with different alkyl chains. The starting material of 2,5-dibromopyrazine is relatively low-cost, thus greatly simplifying the synthesis complexity and reducing the overall synthetic cost. The characterizations of PPy1 and PPy2 are displayed in Figures S1–S4 (Supporting Information).

At first, PPy1 with branched 2-butyloctyl chain was synthesized and its physicochemical properties were investigated. As presented in Figure 1b, the Ultraviolet-visible (UV–vis) absorption spectra of PPy1 exhibits distinct dual absorption peaks, namely the high-energy intramolecular transition (0–1 absorption) peak and the intermolecular transition (0–0 absorption) peak.[46] Note that the maximum absorption peaks (λ_{max}) and relative intensity of 0-0/0-1 absorption peak ($I_{0\text{-}0}/I_{0\text{-}1}$, from 0.90 to 0.91) of PPy1 are almost unchanged from solution to film state, implying the poor intermolecular stacking. The possible reason is the twisting polymer backbone of PPy1, which can be verified by density functional theory (DFT) calculations. As displayed in Figure S5 (Supporting Information), PPy1 displays large dihedral angles between pyrazine unit and two adjacent thiophene units (8.3° and 24.3°). The HOMO/LUMO energy levels of PPy1 were estimated to be −5.62/−3.56 eV afforded by cyclic voltammetry (CV) measurements and the E_g^{opt} of PPy1 derived from its λ_{onset} was 2.07 eV. The results signified that introducing pyrazine unit into polymer backbones could effectively lower the HOMO level of resulting polymer to absorb more high-energy photons, meanwhile, afford a high V_{OC} in corresponding OSCs.

In order to maintain the advantage of wide bandgap whilst conquer the undesired molecular stacking behavior of PPy1, a delicate side chain optimization was further conducted, yielding PPy2 with a smaller *n*-dodecyl chain on the same polymeric backbone. To evaluate the effects of introducing *n*-dodecyl chain on polymer backbone on light absorption, the UV-vis absorption spectra of PPy2 was first measured. As illustrated in Figure 1c, the λ_{max}s of PPy2 in solution are observed at 529 and 562 nm, respectively, slightly red-shifted compared to that of 519 and 553 nm for PPy1. From solution to film state, the $\lambda_{max,0\text{-}0}$ is red-shifted by 6 nm and an increased $I_{0\text{-}0}/I_{0\text{-}1}$ (from 1.05 to 1.11) of PPy2 can be observed, implying more ordered interchain stacking and stronger self-aggregation of PPy2.[46,49] DFT calculation further showed that PPy2 with *n*-dodecyl chain displays smaller dihedral angles between pyrazine unit and connected thiophene units (4.3°, 13.8°), which can promote greater planarity by minimizing distortion in polymer backbone and facilitate molecular ordered assemblies and aggregation property.[37] The E_g^{opt} of PPy2 was determined as 2.02 eV and its HOMO/LUMO energy levels were −5.56/−3.52 eV, respectively. The slightly smaller bandgap may be due to the stronger aggregation of PPy2. It should be noted that the upshifted HOMO energy level of PPy2 is expected to afford a larger driving force for charge dissociation comparing to PPy1 when the same acceptor is employed (Figures 1d and S6, Supporting Information).[50–52]

The same tendency can be observed by analyzing the UV-vis absorption spectra of PPy1 and PPy2 in chlorobenzene solution at different temperatures. As shown in Figure 1e,f, as the temperature increasing from 20 °C to 100 °C, both polymers exhibit the obvious temperature-dependent aggregation properties with the $I_{0\text{-}0}$ gradually weakening and the absorption spectrum gradually blueshifting.[48] Moreover, the 0–0 absorption peaks of PPy1 and PPy2 disappeared at 60 °C and 80 °C, respectively, which further proves the stronger aggregation of PPy2 than PPy1 even in solutions. These findings are consistent with the conclusion that PPy2 exhibits more ordered and tighter π–π stacking than PPy1, which would be unveiled by grazing-incidence wide-angle X-ray scattering (GIWAXS) and discussed detailed below.

The excellent dielectric property of organic materials, which is affected by multiple structurally determining factors,[53–55] will be favor of improving charge dynamics in OSCs, thereby resulting in a high FF and short-circuit current density (J_{SC}). Therefore, the relative dielectric constants (ε_r) of PPy1 and PPy2 were measured (Figures 1g and S7a and Table S1, Supporting Information). In neat films, PPy2 has a higher ε_r of 3.47 than that of 2.66 for PPy1. The enhanced ε_r of PPy2 may be ascribed to its more planar conjugate backbone and superior self-aggregation, which will contribute to the facilitated charge transfer/transport dynamics in OSCs. Note that the improved charge transport of PPy2 has been further verified by its larger hole mobility of 2.16×10^{-4} $cm^2\ V^{-1}\ s^{-1}$ in neat film, while the hole mobility of PPy1 is only 1.32×10^{-4} $cm^2\ V^{-1}\ s^{-1}$ (Figure S7b, Supporting Information). These results substantiate that the different alkyl chains on polymeric backbone have a significant influence on their structural planarity and physicochemical properties. Moreover, the corresponding number-averaged molecular weights (Mn) of PPy1 and PPy2 were estimated to be 55.1 and 56.5 kDa, respectively, by using the gel-permeation chromatography (GPC) measurement with trichlorobenzene as eluent at 150 °C. In addition, the decomposition temperatures (T_d, with 5% weight loss) of PPy1 and PPy2 are both >379 °C according to the thermos-gravimetric analysis (TGA), indicating the excellent thermal stability of polymers (Figure S8, Supporting Information). The corresponding data of PPy1 and PPy2 have been listed in Table S2 (Supporting Information) for a clear presentation.

2.2. Photovoltaic Performances

The excellent aggregation property and enlarged ε_r of PPy2 are expected to have a positive impact on its photovoltaic parameters. Thus, OSCs using PPy1 and PPy2 as the polymer donor were fabricated with a device architecture of ITO/PEDOT:PSS/active layer/PNDIT-F3N/Ag. A wide bandgap acceptor of F-ThCl was chosen to blend with PPy1 and PPy2 in order to achieve an

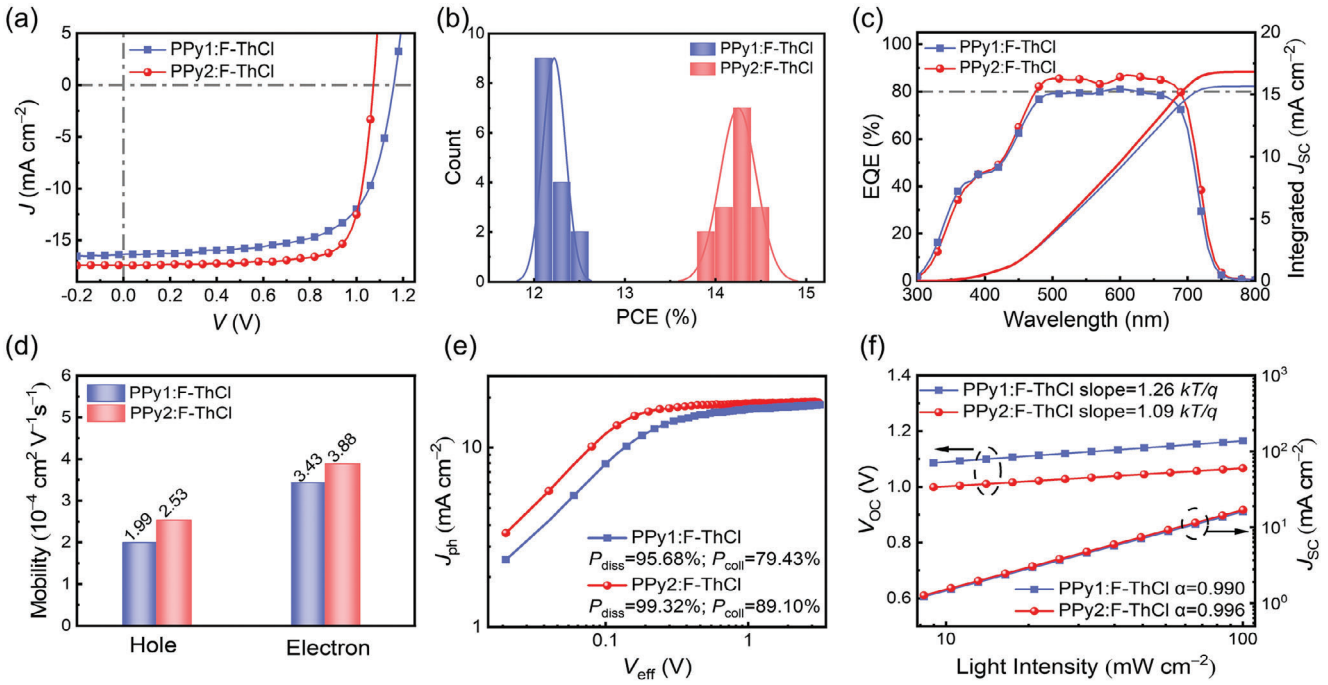

Figure 2. a) *J–V* curves. b) The histogram of PCEs counted by 15 devices. c) EQE spectra and integral J_{SC} values. d) The electron and hole mobility. e) $J_{ph}-V_{eff}$ curves. f) Light intensity dependence of V_{OC} and J_{SC} for PPy1:F-ThCl and PPy2:F-ThCl based OSCs.

efficient OSCs that possess a large V_{OC}.[41] The detailed device optimization was given in Supporting Information (Tables S3 and S5, Supporting Information) and the optimal current density-voltage (*J–V*) characteristics of PPy1- and PPy2-based OSCs were depicted in **Figure** 2a and summarized in **Table** 1.

The optimal PPy2:F-ThCl based OSC gives an outstanding PCE of 14.50%, with a V_{OC} of 1.073 V, a J_{SC} of 17.40 mA cm^{-2} and an FF of 77.66%, significantly better than that of 12.52% for PPy1:F-ThCl with a slightly higher V_{OC} of 1.160 V, a J_{SC} of 16.35 mA cm^{-2} but dramatically inferior FF of 66.03%. As shown in Figure 2b, the average PCEs for PPy2-based devices are obviously higher than PPy1-based devices, demonstrated by the efficiency distribution histogram for 15 distinct devices, which advances among the ranks of OSCs with V_{OC} over 1 V (Table S6, Supporting Information). Moreover, the marginally elevated V_{OC} of PPy1-based OSCs is related to the lower HOMO energy level of PPy1. According to the external quantum efficiency (EQE) spectra (Figure 2c), the integrated current densities are calculated to be 15.74 and 16.92 mA cm^{-2} for the PPy1:F-ThCl and PPy2:F-ThCl devices, respectively, which match well with the J_{SC} given by *J–V* tests (within 4% error range). Note that the higher integrated current density of PPy2-based device is caused by its overall >80% EQE responses in the range of 450–700 nm, which matches well with the light absorption range of the blended films (Figure S9, Supporting Information). This phenomenon is likely due to enhanced exciton dissociation resulting from a comparatively large driving force, as well as facilitated charge transport supported by more suitable blended morphology (would discussed below).[48,56] Furthermore, the markedly enhanced FF for PPy2-based devices should be attributed to improved charge transport dynamics.[57] Therefore, the charge mobility was evaluated through the space-charge limited current (SCLC) method and the electron/hole mobilities (μ_e/μ_h) of PPy1:F-ThCl and PPy2:F-ThCl were 3.43/1.99 and 3.88/2.53 × 10^{-4} cm^2 V^{-1}s^{-1}, equivalent to the μ_e/μ_h ratios of 1.72 and 1.53, respectively (Figure 2d and S10, Supporting Information).

To verify the above discussion, the exciton dissociation efficiency (P_{diss}) and charge collection efficiency (P_{coll}) were first evaluated. As shown in Figure 2e, the values of P_{diss}/P_{coll} can be estimated as 99.32%/89.10% for PPy2:F-ThCl based devices, much better than that of 95.68%/79.43% for PPy1:F-ThCl, which ought to partially explain the higher EQE response of the PPy2-based

Table 1. Photovoltaic parameters of PPy1:F-ThCl and PPy2:F-ThCl based OSCs.[a)]

Active layers	V_{OC} [V]	J_{SC} [mA cm^{-2}]	Cal. J_{SC}[b)] [mA cm^{-2}]	FF [%]	PCE [%]
PPy1:F-ThCl	1.160 (1.157 ± 0.002)	16.35 (16.18 ± 0.08)	15.74	66.03 (65.24 ± 0.41)	12.52 (12.22 ± 0.13)
PPy2:F-ThCl	1.073 (1.070 ± 0.004)	17.40 (17.23 ± 0.14)	16.92	77.66 (77.25 ± 0.85)	14.50 (14.25 ± 0.20)

[a)] The average values obtained from 15 independent devices; [b)] Current densities derived from EQE curves.

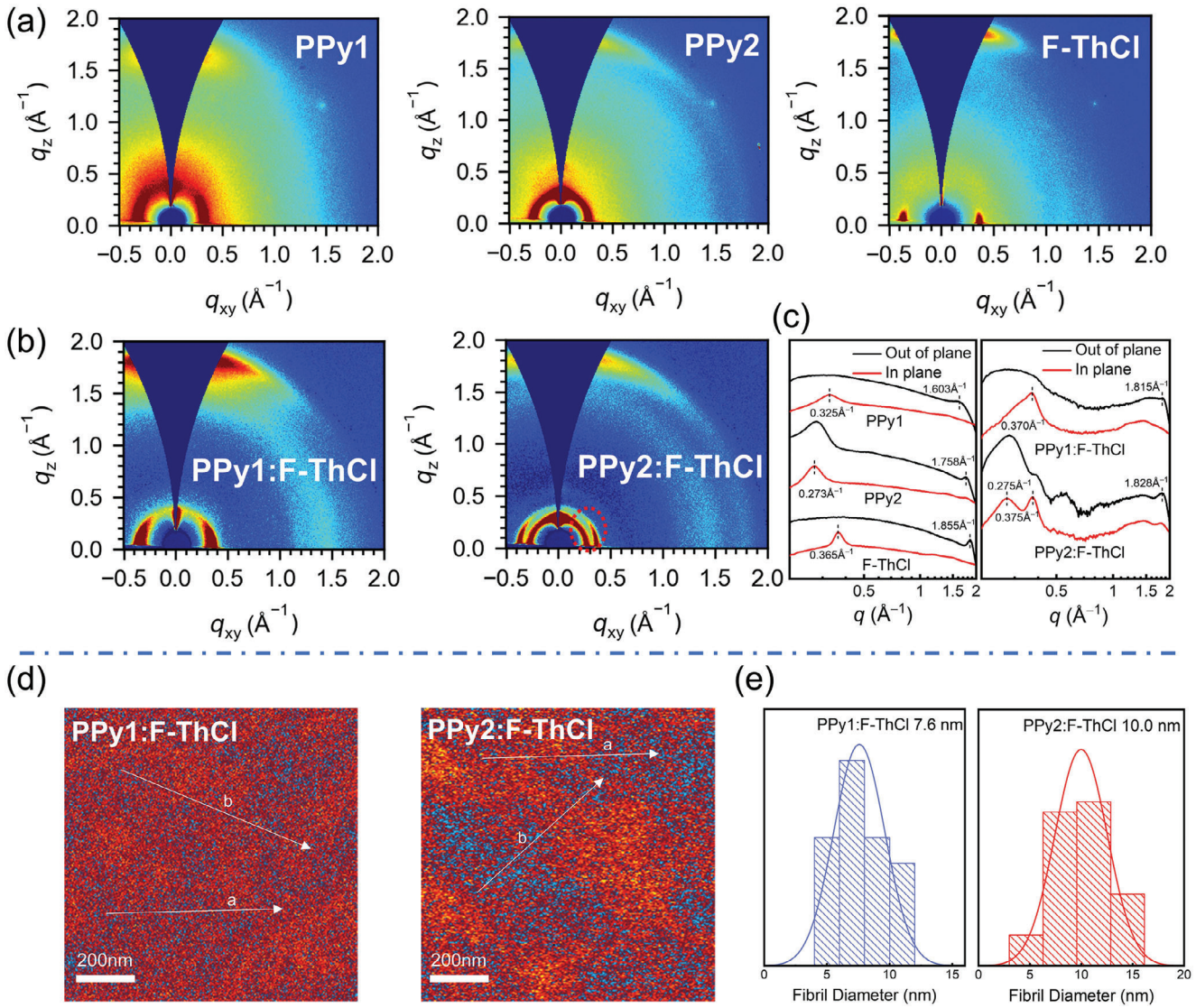

Figure 3. a,b) 2D-GIWAXS patterns and c) 1D scattering profiles of PPy1, PPy2, and F-ThCl neat and blended films. d) AFM-IR images recorded at 2216 cm^{-1} of PPy1:F-ThCl and PPy2:F-ThCl blended films. e) The statistical distribution of fibril diameter.

device. Meanwhile, the improved P_{diss} should be ascribed to the relatively larger driving force for exciton splitting between PPy2 and F-ThCl. Moreover, the higher photoluminescence quenching yield (η_{PLQY}) of 95.18% for PPy2-based device, compared with that of 73.85% for PPy1-based device, also proves its superior exciton dissociation of PPy2-based OSC (Figure S11, Supporting Information). In addition, a relatively faster charge extraction time (0.29 µs) by fitting the transient photocurrent (TPC) decay curves and a longer charge lifetime (91.82 µs) by fitting the transient photovoltage (TPV) decay curves can be evaluated for PPy2-based devices, comparing to that of PPy1-based devices (charge extraction time: 0.43 µs, charge lifetime: 75.29 µs), which suggests more efficient charge extraction and weaker charge recombination in PPy2 system (Figure S12, Supporting Information). The light intensity dependence of J_{SC} and V_{OC} in Figure 2f show the S/(kT/q) values for PPy1 and PPy2-based OSCs are 1.26 and 1.09 and the α for PPy1 and PPy2-based OSCs are 0.990 and 0.996, respectively. These results indicate charge recombination of PPy2-based system is more effectively suppressed comparing to that of PPy1, which is in accordance with the TPV results. In contrast, the PPy2-based device with stronger self-aggregation property and enlarged dielectric property could well improve charge dissociation/transport and thus increase J_{SC} and FF. The detailed photodynamic parameters can be found in Table S7 (Supporting Information).

2.3. Morphology and Energy Losses Analysis

To further understand the effects of introducing pyrazine and different alkyl chains on polymeric backbone on molecular aggregation and packing orientation in neat and blended films, GIWAXS measurement was performed. As demonstrated in **Figure 3a–c**, both PPy1 and PPy2 neat films show an effective face-on

orientation of molecular packing, identified by the strong (010) diffraction peaks at 1.603 and 1.758 Å^{-1} in out-of-plane (OOP) direction, the pronounced (100) diffraction peaks at 0.325 and 0.273 Å^{-1} in in-plane (IP) direction, respectively. And PPy2 neat film shows a strong (010) diffraction peak with a little π–π stacking distance of 3.57 Å in OOP direction due to its more planar conjugated backbone, while the PPy1 neat film gives a weak (010) diffraction peak with a π-π stacking distance of 3.92 Å. Moreover, PPy2 neat film displays a larger crystal coherence length (CCL) of 27.45 Å than that of PPy1 (17.24 Å), suggesting the more ordered intermolecular packing of PPy2. After blending with F-ThCl, the favorable face-on orientation could be well preserved in the blended films, which facilitates effective charge transport in vertical direction.[58] Note that two distinct (100) diffraction peaks at 0.275 and 0.375 Å^{-1} appear in IP direction of PPy2:F-ThCl blended film, corresponding to the (100) diffraction peak at 0.273 and 0.365 Å^{-1} in PPy2 and F-ThCl neat films, respectively, which suggests the molecular stacking of neat films could be well retained in blended film. These results indicate that the tighter π-π packing and higher domain purity in PPy2:F-ThCl blended film comparing to PPy1:F-ThCl are favorable to achieve better charge transport performance, thus afford a much larger J_{SC} and FF in PPy2-based OSCs.

Meanwhile, atomic force microscopy based infrared spectroscopy (AFM-IR) was used to explore the nanoscale morphology and chemical components of blended films.[59,60] In the height images, both PPy1- and PPy2-based blended films exhibit a uniform and relative smooth surface morphology, where the root-mean-square (RMS) are 0.57 and 0.85 nm respectively (Figure S13, Supporting Information). We characterized the blended films signal at 2216 cm^{-1}, matching with the stretching vibration of the C≡N bond of F-ThCl. As displayed in Figure 3d, the uniform distributions with proper domain purity in PPy1- and PPy2-based blended films are observed. And PPy2:F-ThCl blended film exhibits a higher acceptor domain purity than PPy1:F-ThCl, which should be attributed to the stronger self-aggregation property and tighter molecular packing of PPy2. Simultaneously, a statistical size evaluation of nanofibers was carried out and the result showed that PPy2-based blended film had a slightly larger size of 10.0 nm comparing to that of 7.6 nm for PPy1 (Figure 3e). In addition, contact angles and resulting Flory-Huggins interaction parameters (χ) for corresponding donor and acceptor were further investigated.[50] As presented in Figure S14 and Table S8 (Supporting Information), the slightly larger $\chi_{D:A}$ for PPy2:F-ThCl (0.41) than PPy1:F-ThCl (0.17) indicates lower D/A miscibility and higher domain purity in PPy2-based blended film, which corresponds well to its larger nanofiber size. All the results above manifest that introducing pyrazine unit and delicately adjusting alkyl chains on polymeric backbone could well improve molecular aggregation, dielectric property and molecular packing, thereby leading to more effective charge transport performance and excellent photovoltaic efficiencies.

Meanwhile, the energy loss (E_{loss}) of PPy1- and PPy2-based devices were evaluated according to the Shockley-Queisser (SQ) theory. The detailed calculation method and corresponding data were summarized in Supporting information. As illustrated in Table S9 and Figure S15 (Supporting Information), PPy1-based device exhibits lower E_{loss} than that of PPy2 (PPy1: 0.576 eV, PPy2: 0.662 eV), especially for the non-radiative recombination energy loss (ΔE_3, PPy1: 0.220 eV, PPy2: 0.277 eV). These results substantiate that the different alkyl chains on polymeric backbone have a significant influence on E_{loss} of pyrazine polymers. Thereby it is expected to minimize the E_{loss} and enhance V_{OC} of OSCs through further delicately adjusting alkyl chains on pyrazinyl polymeric backbone.

2.4. Fabrication of Tandem Devices

Due to relatively high V_{OC} and outstanding FF, the PPy2:F-ThCl based device exhibits great potential in preparation of high-performance tandem devices. To realize the collaborative utilization of absorption spectrum with the front cell and make full use of low-energy photons, the suitable rear cell was first chosen. Based on the previously proposed semi-empirical model analysis, E_{loss} has a huge impact on the PCEs of TOSCs.[17] Therefore, the emergence of Y-series molecules with low E_{loss} (<0.55 eV) and infrared absorption brings new options for high efficiency rear cell materials. With this, CH1007 was screened as the rear cell material, where the absorption spectrum is further red-shifted to 950 nm and the E_{loss} is reduced to below 0.50 eV.[26] When blending with polymer donor PM6,[30] the optimal PM6:CH1007 based OSC gives a PCE of 16.79% with a V_{OC} of 0.830 V, a J_{SC} of 27.29 mA cm^{-2} and an FF of 74.15%. In order to boost the photovoltaic performance, F-2F with complementary absorption range from 650 to 800 nm was introduced into PM6:CH1007 binary system.[61] With device optimization, the PM6:CH1007:F-2F based device achieves the optimal performance at the D:A ratio of 1:1:0.2, the resulting PCE is 17.61% with an enhanced V_{OC} of 0.845 V, an improved J_{SC} of 28.07 mA cm^{-2}, and an FF of 74.32%. The *J*–*V* characteristics are depicted in Figure S16 (Supporting Information) and summarized in Table S10 (Supporting Information). According to EQE spectra, the integrated current densities increase from 26.26 mA cm^{-2} in the binary system to 26.82 mA cm^{-2} in the ternary system. Note that the absorption spectrum of PM6:CH1007:F-2F based device in the range of 700–950 nm is not overlapped with that of the front cell, which is conducive to utilizing the photons of non-overlapped absorption range to obtain higher J_{SC} for the rear cell.

Subsequently, the tandem device was constructed with PPy2:F-ThCl system as the front cell and PM6:CH1007:F-2F system as the rear cell. The device structure is ITO/ PEDOT:PSS/PPy2:F-ThCl/ZnO nps/PEDOT:PSS/phosphomolybdic acid hydrate (PMA)/PM6:CH1007:F-2F/PNDIT-F3N/Ag (**Figure 4**a,b).[20] As displayed in Figure 4c, the ICL of ZnO nps/PEDOT:PSS/PMA exhibits high transmittance in the absorption range of 300–1100 nm, demonstrating no additional light absorption loss occurs when employed in TOSCs. After that, the sub-cells thickness and the ICL process were carefully optimized. When the thickness values of front and rear sub-cells were 160 and 100 nm, respectively, the most balanced J_{SC} between front and rear sub-cells was obtained. The optimal TOSC outputs an outstanding PCE of 19.35% with a V_{OC} of 1.893 V, a J_{SC} of 13.37 mA cm^{-2}, and an FF of 76.45%. The *J*-*V* curve of tandem device is depicted in Figure 4d and stated in **Table 2**. As depicted in Figure 4e, the integrated J_{SC} obtained from EQE curves of the front and rear cells are 13.23 and 13.23 mA cm^{-2}, respectively, matching well with the J_{SC} afforded by *J*–*V* tests. Concurrently,

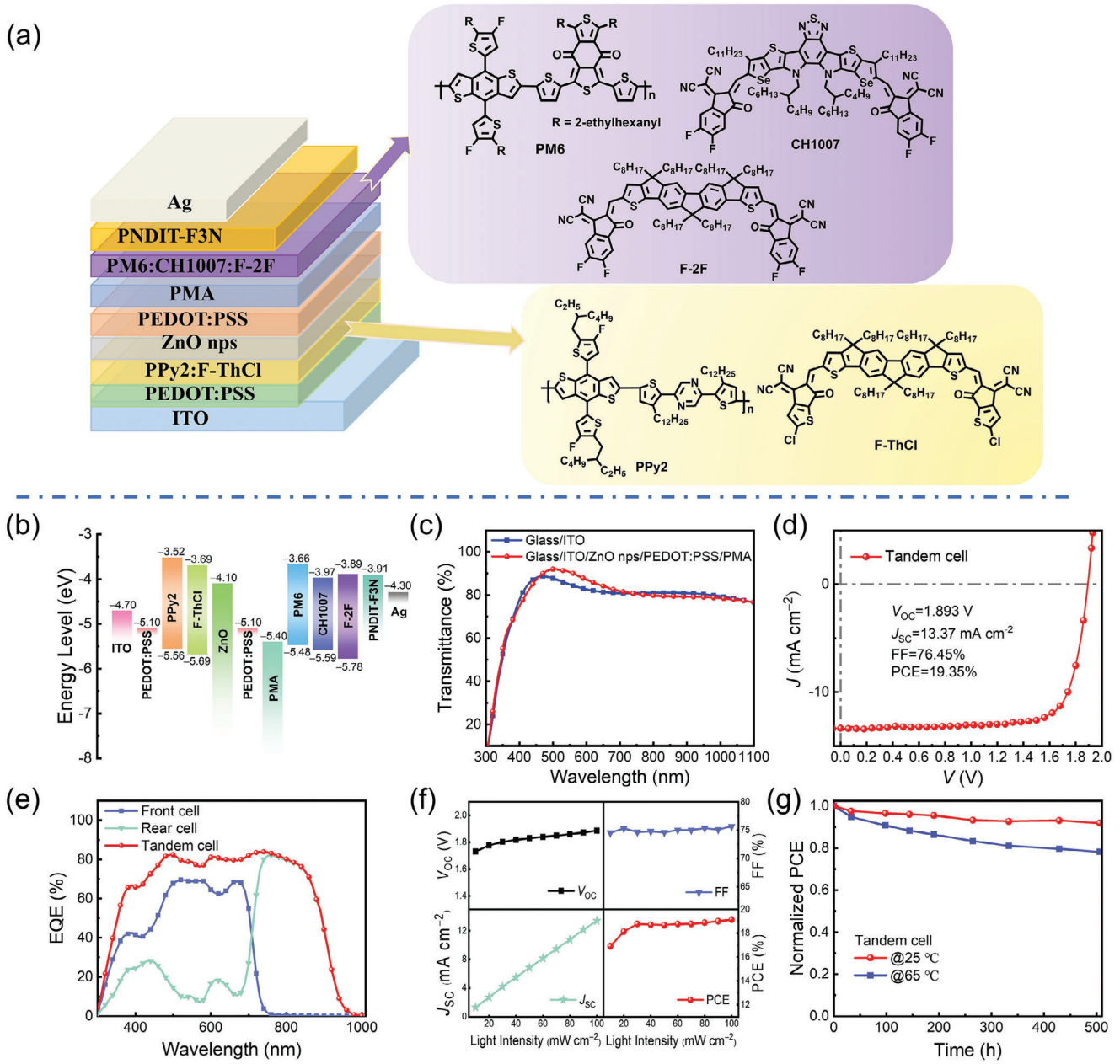

Figure 4. a) The diagram of the tandem device and chemical structures of the corresponding sub-cells. b) Energy level diagram. c) Transmission spectrum of the intermediate junction layer. d) *J-V* curve and e) EQE spectra. f) Variation of photovoltaic parameters under different light intensity. g) PCE variation versus operating time.

Table 2. Photovoltaic parameters of the sub cells and tandem device.[a)]

Active layers	V_{OC} [V]	J_{SC} [mA cm^{-2}]	Cal. J_{SC}[b)] [mA cm^{-2}]	FF [%]	PCE [%]
PPy2:F-ThCl	1.073	17.40	16.92	77.66	14.50
	(1.070 ± 0.004)	(17.23 ± 0.14)		(77.25 ± 0.85)	(14.25 ± 0.20)
PM6:CH1007:F-2F	0.845	28.07	26.82	74.32	17.61
	(0.846 ± 0.003)	(27.93 ± 0.20)		(73.51 ± 0.44)	(17.37 ± 0.15)
Tandem devices	1.893	13.37	13.23/13.23	76.45	19.35
	(1.886 ± 0.004)	(13.31 ± 0.10)		(76.09 ± 0.49)	(19.10 ± 0.17)

[a)] The average values obtained from 10 independent devices; [b)] Current densities derived from EQE curves.

the tandem device shows over 80% EQE spectra response in the range of 400–900 nm.

Besides, the *J*–*V* curves of the tandem device were measured under different light intensities (P_{light}). The results indicate that the PCEs of TOSCs could remain over 17% when the P_{light} varies from 100 to 10 mA cm^{-2}, which suggests the tandem device could function well at varied light intensities (Figure 4f). And the linear relationship between the J_{SC} and P_{light} of TOSCs suggests no serious space charge build-up between the sub-cells and ICL of the tandem device.[14,22] Note that the device stability was also measured, and the PCEs of TOSCs could be maintained ≈90% and ≈80% against its initial PCEs after 500 h under room temperature and heat treatment at 65 °C, respectively (Figure 4g). The superior stability of tandem devices demonstrates its commercial viability in mass manufacture of high-performance TOSCs.

3. Conclusion

In summary, to develop WBG polymer donors with large V_{OC} and high-energy photon absorption for TOSCs, we have constructed two pyrazinyl polymer donors of PPy1 and PPy2, showing both deep HOMO energy levels of ≈−5.60 eV and E_g^{opt}s over 2.0 eV. In spite of an exciting V_{OC} of 1.16 V, PPy1:F-ThCl based OSCs give rise to an inferior PCE of 12.52%, especially a low FF of 66.03%, which should be ascribed to its poor self-aggregation and loose π-π stacking of PPy1 with branched 2-butyloctyl chain. In order to maintain the advantages of V_{OC} whilst conquer the undesired molecular packing of PPy1, a delicate side chain optimization was further conducted, yielding PPy2 with a smaller *n*-dodecyl chain on the same polymeric backbone. As a result, PPy2:F-ThCl based OSCs yield a much improved PCE of 14.50% and FF of 77.66%, along with an excellent V_{OC} of 1.073 V, which is an excellent choice as a front cell of TOSCs. Then the rear cell of PM6:CH1007:F-2F system with λ_{onset} = 950 nm was optimized and achieved a PCE of 17.61%. Subsequently, the TOSCs are constructed and acquire an impressive PCE of 19.35% with an all solution processed ICL. Our work exhibits the great potential of pyrazine units in constructing WBG polymer donors for achieving record-breaking TOSCs.

Supporting Information

Supporting Information is available from the Wiley Online Library or from the author.

Acknowledgements

H.L. and K.M. contributed equally to this work. The authors gratefully acknowledge the financial support from the MoST of China (2022YFB4200400, 2019YFA0705900, and 2023YFE0210400), the NSFC (21935007, 52025033, and 22361132530), the Tianjin city (20JCZDJC00740), and the 111 Project (B12015).

Conflict of Interest

The authors declare no conflict of interest.

Data Availability Statement

The data that support the findings of this study are available from the corresponding author upon reasonable request.

Keywords

alkyl side chain, pyrazine unit, tandem organic solar cell, wide-bandgap polymer donor

Received: June 1, 2024
Revised: July 13, 2024
Published online:

[1] G. Zeng, W. Chen, X. Chen, Y. Hu, Y. Chen, B. Zhang, H. Chen, W. Sun, Y. Shen, Y. Li, F. Yan, Y. Li, *J. Am. Chem. Soc.* **2022**, *144*, 8658.
[2] Z. Xiao, S. Li, J. Liu, X. Chen, Z. Suo, C. Li, X. Wan, Y. Chen, *Sol. RRL* **2024**, *8*, 400206.
[3] X. Huang, X. Ren, Y. Cheng, Y. Zhang, Z. Sun, S. Yang, S. Kim, C. Yang, F. Wu, L. Chen, *Energy Environ. Sci.* **2024**, *17*, 2825.
[4] Z. Liu, Y. Fu, J. Wu, X. Yi, M. Zhao, M. Huang, J. Liu, Z. Xie, *Adv. Funct. Mater.* **2024**, 2401558.
[5] M. Wagner, A. Distler, V. M. Le Corre, S. Zapf, B. Baydar, H.-D. Schmidt, M. Heyder, K. Forberich, L. Lüer, C. J. Brabec, H. J. Egelhaaf, *Energy Environ. Sci.* **2023**, *16*, 5454.
[6] J. Yi, G. Zhang, H. Yu, H. Yan, *Nat. Rev. Mater.* **2024**, *9*, 46.
[7] S. Guan, Y. Li, C. Xu, N. Yin, C. Xu, C. Wang, M. Wang, Y. Xu, Q. Chen, D. Wang, L. Zuo, H. Chen, *Adv. Mater.* **2024**, *36*, 2400342.
[8] Y. Sun, L. Wang, C. Guo, J. Xiao, C. Liu, C. Chen, W. Xia, Z. Gan, J. Cheng, J. Zhou, Z. Chen, J. Zhou, D. Liu, T. Wang, W. Li, *J. Am. Chem. Soc.* **2024**, *146*, 12011.
[9] Z. Yao, X. Cao, X. Bi, T. He, Y. Li, X. Jia, H. Liang, Y. Guo, G. Long, B. Kan, C. Li, X. Wan, Y. Chen, *Angew. Chem., Int. Ed.* **2023**, *62*, 202312630.
[10] J. Fu, Q. Yang, P. Huang, S. Chung, K. Cho, Z. Kan, H. Liu, X. Lu, Y. Lang, H. Lai, F. He, P. W. K. Fong, S. Lu, Y. Yang, Z. Xiao, G. Li, *Nat. Commun.* **2024**, *15*, 1830.
[11] K. Liu, Y. Jiang, G. Ran, F. Liu, W. Zhang, X. Zhu, *Joule* **2024**, *8*, 835.
[12] C. Duan, F. Huang, Y. Cao, *Polym. Chem.* **2015**, *6*, 8081.
[13] Y. Zhang, H. Feng, L. Meng, Y. Wang, M. Chang, S. Li, Z. Guo, C. Li, N. Zheng, Z. Xie, X. Wan, Y. Chen, *Adv. Energy Mater.* **2019**, *9*, 1902688.
[14] Y. Huang, L. Meng, H. Liang, M. Li, H. Chen, C. Jiang, K. Zhang, F. Huang, Z. Yao, C. Li, X. Wan, Y. Chen, *J. Mater Chem.* **2022**, *10*, 11238.
[15] P. Cheng, Y. Liu, S.-Y. Chang, T. Li, P. Sun, R. Wang, H.-W. Cheng, T. Huang, L. Meng, S. Nuryyeva, C. Zhu, K.-H. Wei, B. Sun, X. Zhan, Y. Yang, *Joule* **2019**, *3*, 432.
[16] D. Di Carlo Rasi, R. A. J. Janssen, *Adv. Mater.* **2019**, *31*, 1806499.
[17] L. Meng, Y. Zhang, X. Wan, C. Li, X. Zhang, Y. Wang, X. Ke, Z. Xiao, L. Ding, R. Xia, H.-L. Yip, Y. Cao, Y. Chen, *Science* **2018**, *361*, 1094.
[18] S. Lu, H. Lin, S. Zhang, J. Hou, W. C. H. Choy, *Adv. Energy Mater.* **2017**, *7*, 1701164.
[19] Z. Jia, Q. Ma, Z. Chen, L. Meng, N. Jain, I. Angunawela, S. Qin, X. Kong, X. Li, Y. Yang, H. Zhu, H. Ade, F. Gao, Y. Li, *Nat. Commun.* **2023**, *14*, 1236.
[20] L. Meng, H. Liang, G. Song, M. Li, Y. Huang, C. Jiang, K. Zhang, F. Huang, Z. Yao, C. Li, X. Wan, Y. Chen, *Sci. China Chem.* **2023**, *66*, 808.
[21] Z. Zheng, J. Wang, P. Bi, J. Ren, Y. Wang, Y. Yang, X. Liu, S. Zhang, J. Hou, *Joule* **2022**, *6*, 171.
[22] J. Wang, Z. Zheng, P. Bi, Z. Chen, Y. Wang, X. Liu, S. Zhang, X. Hao, M. Zhang, Y. Li, J. Hou, *Natl. Sci. Rev.* **2023**, *10*, nwad085.
[23] J. Wang, Y. Cui, Z. Chen, J. Zhang, Y. Xiao, T. Zhang, W. Wang, Y. Xu, N. Yang, H. Yao, X.-T. Hao, Z. Wei, J. Hou, *J. Am. Chem. Soc.* **2023**, *145*, 13686.
[24] Z. Jia, S. Qin, L. Meng, Q. Ma, I. Angunawela, J. Zhang, X. Li, Y. He, W. Lai, N. Li, H. Ade, C. J. Brabec, Y. Li, *Nat. Commun.* **2021**, *12*, 178.

[25] J. Yuan, Y. Zhang, L. Zhou, G. Zhang, H.-L. Yip, T.-K. Lau, X. Lu, C. Zhu, H. Peng, P. A. Johnson, M. Leclerc, Y. Cao, J. Ulanski, Y. Li, Y. Zou, *Joule* **2019**, *3*, 1140.
[26] F. Lin, K. Jiang, W. Kaminsky, Z. Zhu, A. K. Y. Jen, *J. Am. Chem. Soc.* **2020**, *142*, 15246.
[27] G. Song, W. Feng, Y. Li, H. Liang, Z. Li, B. Kan, X. Wan, Z. Yao, C. Li, Y. Chen, *Chem. Commun.* **2023**, *59*, 10307.
[28] C. Li, J. Zhou, J. Song, J. Xu, H. Zhang, X. Zhang, J. Guo, L. Zhu, D. Wei, G. Han, J. Min, Y. Zhang, Z. Xie, Y. Yi, H. Yan, F. Gao, F. Liu, Y. Sun, *Nat. Energy* **2021**, *6*, 605.
[29] J. Wang, M. Zhang, J. Lin, Z. Zheng, L. Zhu, P. Bi, H. Liang, X. Guo, J. Wu, Y. Wang, L. Yu, J. Li, J. Lv, X. Liu, F. Liu, J. Hou, Y. Li, *Energy Environ. Sci.* **2022**, *15*, 1585.
[30] M. Zhang, X. Guo, W. Ma, H. Ade, J. Hou, *Adv. Mater.* **2015**, *27*, 4655.
[31] Q. Liu, Y. Jiang, K. Jin, J. Qin, J. Xu, W. Li, J. Xiong, J. Liu, Z. Xiao, K. Sun, S. Yang, X. Zhang, L. Ding, *Sci. Bull.* **2020**, *65*, 272.
[32] R. Ma, T. Liu, Z. Luo, Q. Guo, Y. Xiao, Y. Chen, X. Li, S. Luo, X. Lu, M. Zhang, Y. Li, H. Yan, *Sci. China Chem.* **2020**, *63*, 325.
[33] J. Qin, L. Zhang, C. Zuo, Z. Xiao, Y. Yuan, S. Yang, F. Hao, M. Cheng, K. Sun, Q. Bao, Z. Bin, Z. Jin, L. Ding, *J. Semicond.* **2021**, *42*, 010501.
[34] D. Xie, Y. Zhang, X. Yuan, Y. Li, F. Huang, Y. Cao, C. Duan, *Adv. Funct. Mater.* **2023**, *33*, 2212601.
[35] B. Yin, S. Pang, Z. Chen, W. Deng, Z. Liu, C. Duan, F. Huang, Y. Cao, *Energy Environ. Sci.* **2022**, *15*, 4789.
[36] X. Yuan, Y. Zhao, D. Xie, L. Pan, X. Liu, C. Duan, F. Huang, Y. Cao, *Joule* **2022**, *6*, 647.
[37] T. Zhang, C. An, Y. Cui, J. Zhang, P. Bi, C. Yang, S. Zhang, J. Hou, *Adv. Mater.* **2022**, *34*, 2105803.
[38] C. Sun, F. Pan, H. Bin, J. Zhang, L. Xue, B. Qiu, Z. Wei, Z.-G. Zhang, Y. Li, *Nat. Commun.* **2018**, *9*, 743.
[39] J. Wu, Q. Fan, M. Xiong, Q. Wang, K. Chen, H. Liu, M. Gao, L. Ye, X. Guo, J. Fang, Q. Guo, W. Su, Z. Ma, Z. Tang, E. Wang, H. Ade, M. Zhang, *Nano Energy* **2021**, *82*, 105679.
[40] D. Qian, Z. Zheng, H. Yao, W. Tress, T. R. Hopper, S. Chen, S. Li, J. Liu, S. Chen, J. Zhang, X.-K. Liu, B. Gao, L. Ouyang, Y. Jin, G. Pozina, I. A. Buyanova, W. M. Chen, O. Inganäs, V. Coropceanu, J.-L. Bredas, H. Yan, J. Hou, F. Zhang, A. A. Bakulin, F. Gao, *Nat. Mater.* **2018**, *17*, 703.
[41] F. Bai, J. Zhang, A. Zeng, H. Zhao, K. Duan, H. Yu, K. Cheng, G. Chai, Y. Chen, J. Liang, W. Ma, H. Yan, *Joule* **2021**, *5*, 1231.
[42] J. Cao, L. Yi, L. Zhang, Y. Zou, L. Ding, *J. Mater Chem.* **2023**, *11*, 17.
[43] K. Nakano, Y. Chen, B. Xiao, W. Han, J. Huang, H. Yoshida, E. Zhou, K. Tajima, *Nat. Commun.* **2019**, *10*, 2520.
[44] S. Pang, Z. Wang, X. Yuan, L. Pan, W. Deng, H. Tang, H. Wu, S. Chen, C. Duan, F. Huang, Y. Cao, *Angew. Chem., Int. Ed.* **2021**, *60*, 8813.
[45] G. P. Kini, J. Y. Choi, S. J. Jeon, I. S. Suh, D. K. Moon, *Polym. Chem.* **2019**, *10*, 4459.
[46] L. Zhou, L. Meng, J. Zhang, C. Zhu, S. Qin, I. Angunawela, Y. Wan, H. Ade, Y. Li, *Adv. Funct. Mater.* **2022**, *32*, 2109271.
[47] L. Guo, K. Liu, X. Tan, X. Wang, J. Huang, Z. Wei, G. Chen, *Macromolecules* **2021**, *54*, 10758.
[48] J. Ren, S. Zhang, P. Bi, Z. Chen, T. Zhang, J. Wang, L. Ma, J. Li, J. Hou, *J. Mater Chem.* **2022**, *10*, 25595.
[49] X. Cao, J. Guo, Z. Li, X. Bi, H. Liang, Z. Xiao, Y. Guo, X. Jia, Z. Xu, K. Ma, Z. Yao, B. Kan, X. Wan, C. Li, Y. Chen, *ACS Energy Lett.* **2023**, *8*, 3494.
[50] H. Liang, X. Bi, H. Chen, T. He, Y. Lin, Y. Zhang, K. Ma, W. Feng, Z. Ma, G. Long, C. Li, B. Kan, H. Zhang, O. A. Rakitin, X. Wan, Z. Yao, Y. Chen, *Nat. Commun.* **2023**, *14*, 4707.
[51] L. Perdigón-Toro, H. Zhang, A. Markina, J. Yuan, S. M. Hosseini, C. M. Wolff, G. Zuo, M. Stolterfoht, Y. Zou, F. Gao, D. Andrienko, S. Shoaee, D. Neher, *Adv. Mater.* **2020**, *32*, 1906763.
[52] M. Azzouzi, N. P. Gallop, F. Eisner, J. Yan, X. Zheng, H. Cha, Q. He, Z. Fei, M. Heeney, A. A. Bakulin, J. Nelson, *Energy Environ. Sci.* **2022**, *15*, 1256.
[53] M. P. Hughes, K. D. Rosenthal, N. A. Ran, M. Seifrid, G. C. Bazan, T.-Q. Nguyen, *Adv. Funct. Mater.* **2018**, *28*, 1801542.
[54] W. Jiang, H. Jin, M. Babazadeh, A. S. Loch, A. Raynor, N. Mallo, D. M. Huang, X. Jiao, W. L. Tan, C. R. McNeill, P. L. Burn, P. E. Shaw, *Adv. Funct. Mater.* **2022**, *32*, 2104259.
[55] H. Liang, H. Chen, P. Wang, Y. Zhu, Y. Zhang, W. Feng, K. Ma, Y. Lin, Z. Ma, G. Long, C. Li, B. Kan, Z. Yao, H. Zhang, X. Wan, Y. Chen, *Adv. Funct. Mater.* **2023**, *33*, 2301573.
[56] A. C. Jakowetz, M. L. Böhm, A. Sadhanala, S. Huettner, A. Rao, R. H. Friend, *Nat. Mater.* **2017**, *16*, 551.
[57] A. Melianas, V. Pranculis, D. Spoltore, J. Benduhn, O. Inganäs, V. Gulbinas, K. Vandewal, M. Kemerink, *Adv. Energy Mater.* **2017**, *7*, 1700888.
[58] Z. Wang, Y. Zhang, J. Zhang, Z. Wei, W. Ma, *Adv. Energy Mater.* **2016**, *6*, 1502456.
[59] M. Zhang, L. Zhu, T. Hao, G. Zhou, C. Qiu, Z. Zhao, N. Hartmann, B. Xiao, Y. Zou, W. Feng, H. Zhu, M. Zhang, Y. Zhang, Y. Li, T. P. Russell, F. Liu, *Adv. Mater.* **2021**, *33*, 2007177.
[60] X. Xu, Y. Li, Q. Peng, *Adv. Mater.* **2022**, *34*, 2107476.
[61] X. Ke, L. Meng, X. Wan, M. Li, Y. Sun, Z. Guo, S. Wu, H. Zhang, C. Li, Y. Chen, *J. Mater Chem.* **2020**, *8*, 9726.